ISSN0379-301X

UNIVERSITE LIBRE DE BRUXELLES - VRIJE UNIVERSITEIT BRUSSEL

INTER-UNIVERSITY INSTITUTE FOR HIGH ENERGIES

RAPIDITY AND TRANSVERSE MOMENTUM STRUCTURE IN π^+ AND K^+ COLLISIONS WITH Al AND Au NUCLEI AT 250 GeV/C

NA22 Collaboration

Universities of Brussels (ULB-VUB)
Pleinlaan, 2
1050 Brussels

November 1990
IIHE-90.02

Rapidity and Transverse Momentum Structure in π^+ and K^+ Collisions with Al and Au Nuclei at 250 GeV/c

EHS–NA22 Collaboration

Antwerp/Brussels[a]–Berlin(Zeuthen)[b]–Helsinki[c]– Krakow[d]– Moscow[e]– Nijmegen[f]–Rio de Janeiro[g]–Serpukhov[h]–Tbilisi[i]–Warsaw[j]–Yerevan[k]

N.M. AGABABYAN[k], I.V. AJINENKO[h], Yu.A. BELOKOPYTOV[h], H. BOETTCHER[b], F. BOTTERWECK[f], M. CHARLET[a,1] P.V. CHLIAPNIKOV[h], F. CRIJNS[f], A. DE ROECK[a,2], E.A. DE WOLF[a,3], K. DZIUNIKOWSKA[d], A.M.F. ENDLER[g], A. ESKREYS[d], Z.C. GARUTCHAVA[i], P. van HAL[f,4], R.Sh. HAKOBYAN[k], T. HAUPT[f,5] W. KITTEL[f], D. KISIELEWSKA[d], B.B. LEVCHENKO[e], B. MACHOWSKI[d], F. MEIJERS[f,6], A.B. MICHALOWSKA[a], V.I. NIKOLAENKO[h], K. OLKIEWICZ[d], F.K. RIZATDINOVA[e], V.M. RONJIN[h], A.M. RYBIN[h], H.M.T. SAARIKKO[c], L. SCHOLTEN[f,7], L.N. SMIRNOVA[e], J. STEPANIAK[j], O.G. TCHIKILEV[h], V.A. UVAROV[h], F. VERBEURE[a], R. WISCHNEWSKI[b],

[a]Dept. of Physics, Universitaire Instelling Antwerpen, B-2610 Wilrijk, and Interuniversity Institute for High Energies, B-1050 Brussels, Belgium

[b]Institut für Hochenergiephysik, D-O-1615 Berlin-Zeuthen, German Democratic Republic

[c]Department of High Energy Physics, University of Helsinki, SF-00170 Helsinki, Finland

[d]Institute of Physics and Nuclear Techniques of the Academy of Mining and Metallurgy and Institute of Nuclear Physics, PL-30055 Krakow, Poland; partially supported by grants from CPBP 01.06 and 01.09

[e]Moscow State University, SU-119899 Moscow, USSR

[f]University of Nijmegen and NIKHEF-H, NL-6525 ED Nijmegen, The Netherlands

[g]Centro Brasileiro de Pesquisas Fisicas, BR-22290 Rio de Janeiro, Brazil

[h]Institute for High Energy Physics, SU-142284 Serpukhov, USSR

[i]Institute of High Energy Physics, Tbilisi State University, SU-380086 Tbilisi, USSR

[j]University of Warsaw and Institute of Nuclear Problems, PL-00681 Warsaw, Poland; partially supported by grants from CPBP 01.06 and 01.09

[k]Institute of Physics, SU-375036 Yerevan, USSR

[1]SCIENCE Research Fellow, EEC, Brussels, Belgium

[2]Onderzoeker IIKW, Brussels, Belgium, now at MPI, München

[3]Bevoegdverklaard Navorser NFWO, Belgium

[4]Now with Ericsson Telecommunicatie B.V., Rijen, The Netherlands

[5]Now at Syracuse University, Syracuse NY 13244–1130, USA

[6]Now at CERN, Geneva, Switzerland

[7]Now at Pandata, Rijswijk, The Netherlands

Abstract

An analysis is presented of the rapidity and transverse momentum distributions and of the nuclear stopping power in collisions of π^+ and K^+ mesons with Al and Au nuclei at 250 GeV/c. The experimental results are compared to predictions of the Additive Quark Model and the Dual Parton Model. The AQM offers an overall consistent description of the data in this experiment. The DPM reproduces reasonably well the rapidity spectra in the central and projectile fragmentation regions, but fails to describe the nuclear stopping power.

1 Introduction

Nuclei as targets offer unique experimental conditions for the study of interactions between hadrons, not present in elementary interactions on protons or neutrons. Nowhere except inside a nucleus are the strongly interacting particles so densely packed in space and are the target nucleons within the range of their mutual strong forces. It is now generally accepted that an interaction with a nucleus can, to a good approximation, be regarded as a superposition of consecutive collisions of an incident particle (or its constituents) with the nucleons encountered on its path through the nucleus. In such a picture, hadron interactions with nuclei are expected to add new insight into the nature of the strong interaction and, in particular, reveal differences in characteristics for hadrons produced off strongly bound and free nucleons.

In this paper we use the "multiple collision" concept as the main guideline for our analysis. In particular, we compare the data to two models based on this concept: the Dual Parton Model (DPM) of Capella et al. [1] and the Additive Quark Model (AQM) of Białas et al. [2]. The 4π angular coverage of produced particles and the reliable identification of low energy protons in our experiment, make it possible to verify this concept of multiple collisions and to distinguish between the models. In particular, it is interesting to address the question whether an interaction with a nucleus is a simple incoherent superposition of collisions with individual free-like nucleons or to point out observations which contradict this picture.

The present results are obtained in our study of π^+ and K^+ collisions with Al and Au nuclei at 250 GeV/c incident meson momentum, the highest energy positive meson beam available so far. The data have been collected with the European Hybrid Spectrometer (EHS) at the CERN SPS by the NA22 collaboration. Due to the insertion of thin aluminum and gold foils inside the Rapid Cycling Bubble Chamber (RCBC), the detection of interactions with hydrogen as well as with Al and Au nuclei became possible in a single experiment, thus subject to identical experimental biases. Published data on kaon interactions with nuclei in the few hundred GeV energy range are still rather scarce (see [3] for a review). The main advantages of our detector are an active vertex detector and identification of protons with laboratory momentum $p_{\rm lab} < 1.2$ GeV/c.

In previous papers on our Al and Au data [4–5] we presented a detailed analysis of the multiplicity distributions. Here, we concentrate on other general features of these interactions, such as rapidity and transverse momentum distributions and nuclear stopping power.

The paper is organized as follows. Some brief information about the data samples is given in Sect. 2. Rapidity distributions are studied and compared to model predictions in Sect. 3. Results on transverse momenta are given in Sect. 4 and on "nuclear stopping power" in Sect. 5. Our conclusions are summarized in Sect.6.

2 The data sample

The selection of the event and track sample is described in detail in our earlier paper [4]. The main selection criteria are the following :

- the incident particle track is well measured and matches with hits in the upstream wire chambers;
- the reconstructed vertex position is within one of the foils;
- the outgoing tracks are satisfactorily measured and reconstructed; the loss of tracks due to measurement or reconstruction failures is at most one for charged particle multiplicities up to 10, and at most 20% for higher multiplicities;
- the event is not a candidate for a quasi-elastic or coherent interaction;
  - A quasi-elastic event is defined by the following criteria:
    1. the charge multiplicity equals two,
    2. the missing transverse momentum is less than 0.2 GeV/c,
    3. the missing longitudinal momentum is less than 9 GeV/c.
  - A coherent interaction is defined by the requirements that
    1. the charge multiplicity is odd and ≤ 5,
    2. all charged particles have rapidities larger than one, if measured in the meson–nucleon c.m. system.

Multiplicity dependent weights are introduced to correct for the loss of events. The present analysis is based on a total of 7992 interactions passing the selection criteria: 3188 $\pi^+ Al$, 2760 $\pi^+ Au$, 1082 $K^+ Al$ and 962 $K^+ Au$ events. Ionization information is used to identify protons up to 1.2 GeV/c and electrons and positrons up to 200 MeV/c. All unidentified tracks are given the pion mass.

In the picture of multiple collisions, the number ν of projectile collisions inside a nucleus is of primary importance. The average number of projectile collisions for the full samples of hA interactions, is defined as

$$\overline{\nu} = A\frac{\sigma_{hp}^{inel}}{\sigma_{hA}^{inel}}.$$

For more differential analyses, we study in subsequent sections hadron-nucleus interactions as a function of the number n_g of grey protons in the event. These are defined as protons identified from their ionization in the bubble chamber, with velocity $0.2 < \beta < 0.7$ (or equivalently $0.19 < p_{\rm lab} < 0.92$ GeV/c).

3 Rapidity Distributions

3.1 Single Particle Distributions

The c.m. rapidity y is defined as

$$y = \frac{1}{2} \ln \frac{E + p_{||}}{E - p_{||}}, \tag{3.1}$$

where $p_{||}$ is the particle momentum component parallel to the beam axis, calculated in the meson–nucleon cms. In this reference system, the value of rapidity for target nucleons at rest in the laboratory system is $y_0 = -3.14$, both for π^+ and K^+ incident mesons.

The rapidity density distribution

$$\varrho_A(y) = \frac{1}{N_{ev}} \frac{dN}{dy} \tag{3.2}$$

is given in Table 1(a–d) for the four reactions studied, separately for all positive particles, for positive particles excluding identified protons and for negative particles. The distributions are very similar for π^+ and K^+ beams. For illustration, we show in Fig. 1 the rapidity densities for K^+ collisions.

For positive particles (Fig. 1a), a large particle density is observed at large negative y which increases strongly with A, the atomic number of the target nucleus. Much of this enhancement is due to protons, as seen from the distribution (open symbols in Fig. 1a) after exclusion of identified protons. The particle density in the beam fragmentation region ($y > 1$) is the same within errors for Al and Au targets. For negative particles (Fig. 1b), the distributions also coincide in the beam fragmentation region while the density at negative y–values increases with A.

In the approach of consecutive projectile collisions, it is assumed that the first collision leads to a rapidity distribution $a(y)$ and that each consecutive collision adds an identical contribution $b(y)$. For a given value of $\overline{\nu}$ this approach [6] assumes that $\varrho_A(y)$ can be written as

$$\varrho_A(y) = a(y) + (\overline{\nu} - 1) b(y) \tag{3.3}$$

where $b(y)$ is independent of $\overline{\nu}$, but the functions $a(y)$ and $b(y)$ can be *a priori* different for Al and for Au target nuclei.

To determine the functions $a(y)$ and $b(y)$, we divide the total event sample for each target into subsamples with different numbers n_g of grey protons. Using the method of [7], we determine for each subsample the corresponding value of $\overline{\nu}$ and its probability $P_{\overline{\nu}}$. The selected subsamples are listed in Table 2, separately for the Al and Au targets, together with the corresponding number of observed grey protons n_g, the value of $\overline{\nu}$ and the probability $P_{\overline{\nu}}$ of $\overline{\nu}$ collisions. The functions $a(y)$ and $b(y)$

are then fitted using (3.3) and the rapidity distribution of negative particles in each subsample. For this analysis we combine the K^+ and π^+ samples[1]. The condition that the functions $a(y)$ and $b(y)$ be non–negative, is not imposed in the fit.

The results are shown in Fig. 2, where two observations can be made:

- the contribution $a(y)$ from the first collision is centered at larger y values than $b(y)$, in agreement with the assumption that the first collision is of higher energy than subsequent ones, and
- both $a(y)$ and $b(y)$ are similar in shape for Al and Au; they are the same within errors in the forward hemisphere $y > 0$.

One may expect the rapidity density $a(y)$ to be similar to the one observed in elementary non-diffractive π^+p or K^+p collisions, which we denote by $\varrho_p(y)$. The comparison of the two is shown in Fig. 3a. It is remarkable that the general shape is similar and $a(y)$ and $\rho_p(y)$ coincide for $y > 1.5$; $a(y)$ is larger than $\varrho_p(y)$ in the central rapidity region, but smaller in the region $y < -1.5$ for the Au target. The discrepancy between $a(y)$ and $\varrho_p(y)$ is more pronounced for the heavier target. It is not clear whether the differences relative to the M^+p data are related to the simple assumptions underlying (3.3), in particular that $b(y)$ is independent of $\overline{\nu}$, or reflect a physical difference in particle production rate off bound and free nucleons.

The dashed curves in Fig. 3 show the predictions of the DPM[2], which turn out to lie quite close to the rapidity density $\varrho_p(y)$ in elementary collisions, but lead to a $b(y)$ spectrum which is too hard in the beam fragmentation region (Fig. 3b). The model, as used in this paper, neglects cascading in the target and is therefore not expected to describe $b(y)$ at negative y-values.

3.2 Dependence on the Number $\overline{\nu}$ of Projectile Collisions

The characteristic features of the rapidity distribution become more evident if one investigates the ratio $R(y)$ of the rapidity density $\varrho_A(y)$ in nuclear collisions to that in elementary collisions $\varrho_p(y)$ on protons. The corresponding plots are shown for both beam types in Fig. 4a (for all positive particles) and in Fig. 4b (for negative particles), together with the predictions from the DPM. Outside the cascade region the model reproduces the data quite well.

Brick et al. [9] recently published $R(y)$ distributions for all particles and for negative ones in 200 GeV/c π^+, K^+ and proton interactions on Au, Ag and Mg

[1]Wherever we use the combined K^+ and π^+ samples in what follows, we will use the notation "M^+"

[2]To obtain the prediction for $a(y)$ in the DPM, the contribution from all chains except those involving projectile valence quarks was switched off. For $b(y)$, only the contribution from chains involving projectile sea quarks was kept

nuclei, based on statistics which is an order of magnitude smaller than in this work. The distributions in [9] which can be directly compared with our results, agree in shape and, within errors, also in magnitude with our results.

In Fig. 5 we show the ratio $R^-(y) = \varrho_A(y)/\varrho_p(y)$ for negative particles in three different regions of rapidity, as a function of the average number $\overline{\nu}$ of projectile collisions inside the nucleus and, in the target fragmentation region, as a function of the number of observed grey protons n_g, for the two beam types and target nuclei studied.

Since both the AQM and DPM predict R^- in the central region, we first concentrate on the interval $-0.5 < y < 1.0$. In Fig. 5c, the prediction of the DPM is shown as the dashed curve while the arrows indicate the limiting values of $R^-(y)$ for $\overline{\nu} = 1$ and for $\overline{\nu} \to \infty$, following from the AQM. Both models are in fair agreement with the data although the flattening of $R^-(y)$ with increasing $\overline{\nu}$ observed in the data is more in favour of the AQM. Reasonable readjustments of the chosen rapidity interval do not change the above conclusion.

In the beam fragmentation region (Fig. 5d) $R^-(y)$ decreases with increasing $\overline{\nu}$. In the target fragmentation region (Fig. 5a) $R^-(y)$ increases with $\overline{\nu}$, possibly stronger than linearly for the Au target. In Fig. 5b we show the dependence of $R^-(y)$ on n_g, the observed number of grey protons, for $y < -2.5$. Comparison of this figure with Fig. 5a indicates that the target dependence may be less pronounced if $R^-(y)$ is plotted versus n_g. This observation, if confirmed, would imply that the nuclear cascade process is mainly sensitive to the total number of collisions, measured by n_g, rather than to the number of projectile collisions, measured by $\overline{\nu}$.

3.3 Spectator and Wounded Quark Fragmentation in AQM

In the AQM approach, the rapidity density $\varrho_A(y)$ in the meson fragmentation region of meson-nucleus collisions is given by

$$\varrho_A(y) = P_{s_{\overline{q}}}\left[F_{s_{\overline{q}}}(y) + F_{w_q}(y)\right] + P_{s_q}\left[F_{s_q}(y) + F_{w_{\overline{q}}}(y)\right] + P_{ww}\left[F_{w_q}(y) + F_{w_{\overline{q}}}(y)\right] \quad (3.4)$$

where $F_{s_i}(y)$ and $F_{w_i}(y)$ ($i = q$ or $\overline{q}$) are the fragmentation functions of the so-called spectator and wounded quarks in the projectile. A wounded quark is a quark which actively participates in the interaction. P_{s_i} ($i = q$ or $\overline{q}$) and P_{w_i} ($i = q$ or $\overline{q}$) are the probabilities of quark q or antiquark $\overline{q}$ to be a spectator and a wounded quark in the collision, respectively, and P_{ww} is the probability that both quarks in the projectile be wounded[3]. Since, for a given number of collisions $\overline{\nu}$, P_{s_i} and P_{ww} are known [2,8], the fragmentation functions $F_s(y)$ and $F_w(y)$ can be determined from the experimental data at different values of $\overline{\nu}$. Having at our disposal both $\pi^+(u\overline{d})$ and $K^+(u\overline{s})$ as incident particles, one could in principle attempt to find the

[3]For the calculation of P_s and P_{ww} we use the following cross sections: for the π^+-beam $\sigma_{qN} = 0.5\sigma_{\pi N}$ and for the K^+-beam $\sigma_{uN} = \frac{3}{5}\sigma_{Kp}$ and $\sigma_{\overline{s}N} = \frac{2}{5}\sigma_{Kp}$

fragmentation functions of the spectator and wounded quarks of each participating flavour $(u, \overline{d}, \overline{s})$, separately. However, the limited statistics forces us to reduce the number of unknown functions and to assume that $F_{s_q}(y) = F_{s_{\overline{q}}}(y)$ and $F_{w_q}(y) = F_{w_{\overline{q}}}(y)$.

The resulting distributions are shown in Fig. 6 for positive and negative particles from the M^+ sample. Both figures show that the fragmentation of wounded quarks leads to a much softer y spectrum than that of spectator quarks.

The AQM picture allows for a further independent check. The density $\varrho_p(y)$ for π^+ and K^+ collisions with protons should simply be the sum of the spectator and the wounded quark fragmentation functions derived above:

$$\varrho_p(y) = F_s(y) + F_w(y). \tag{3.5}$$

This is shown in Fig. 7. The agreement with the combined data on non-diffractive π^+p and K^+p collisions [10] is indeed quite remarkable, although some deviations are noted in the central region.

4 Transverse Momentum Distributions

In the study of transverse momentum distributions and derived quantities, particular attention must be paid to the contribution of unidentified electrons and positrons from γ-conversions, since these are concentrated in a narrow region at small p_t. As mentioned above, $e^{\pm}$'s are identified in the bubble chamber if their laboratory momentum is less than 200 MeV/c. The contribution from unidentified $e^{\pm}$'s is estimated by Monte Carlo simulation, using the DPM and taking into account the thickness of the foils.

In Tables 3(a–b) we present the corrected transverse momentum distributions, normalized to unity, $g_A(p_t)$, for positive and negative particles in π^+Al, π^+Au, K^+Al and K^+Au collisions. The shape of $g_A(p_t)$ depends very little on the beam type and the K^+ and π^+ samples are again merged in the subsequent analysis. The correction factors, given in Table 3c, strongly differ from zero at small p_t values, particularly for interactions in the gold foil. The results on the Figs. 8–10 are also corrected for unidentified electrons.

The average transverse momentum of negative particles (all rapidities) is plotted in Fig. 8 as a function of n^-, the negative particle multiplicity. At this energy, the M^+p data show a monotonic decrease of $< p_t >$ with increasing number n^- of negative particles while $< p_t >$ is almost constant for the nuclear data.

To study nuclear effects, we consider the ratio $R(p_t)$

$$R(p_t) = \frac{g_A(p_t)}{g_p(p_t)}. \tag{4.6}$$

Here $g_A(p_t)$ is the distribution for the π^+ and K^+ beam data combined and $g_p(p_t)$ is the corresponding p_t distribution in π^+p and K^+p collisions as measured in this experiment [10]. Figs. 9(a–d) show $R(p_t)$ for positive and negative particles and for the two targets separately. In all cases the ratio is larger than unity in the $p_t > 1$ GeV/c region and the relative excess is most pronounced for negative particles and largest for the heaviest target.

Concentrating on negative particles, we show in Fig. 9(e–h) the data separately for particles with positive and negative c.m. rapidity. In the region of $p_t > 1$ GeV/c, R is larger than one in both hemispheres and for both targets. At small p_t-values, the ratio is less than one in the forward and larger than one in the backward hemisphere. Within the experimental errors, no A-dependence of the effects is observed. The excess of particles with higher p_t in collisions with nuclei finds a natural explanation as a consequence of multiple collisions of particles inside the nucleus.

In Fig. 10 we plot the average transverse momentum $< p_t >$ of negative particles as a function of Feynman x_F. In the forward hemisphere, $< p_t >$ is the same for meson-proton and meson-Al interactions but is considerably larger in meson-Au interactions. In the region $x_F < -0.15$, where intranuclear cascading plays a dominant rôle, the $< p_t >$ is smaller in both meson-nucleus interactions than in elementary collisions.

In a multiple collision picture, hadrons are believed to originate from a number of "elementary" collisions. Hadron production in the latter is characterized by short range order which implies strong correlations among particles at small rapidity differences and local compensation of transverse momentum. However, for multiple collisions inside a nuclear target, correlations among particles in a small rapidity window are expected to be weakened due to random superposition[4]. To investigate this effect in the data, we consider the variable $< (\sum_i \vec{p}_{ti})^2 >$, the squared sum of the transverse momentum vectors in an event, averaged over all events with charge multiplicity n. In the absence of p_t-correlations, and neglecting transverse momentum conservation, one obtains the relation

$$< (\sum_{i=1}^{n} \vec{p}_{t_i})^2 >= n < p_t^2 > . \tag{4.7}$$

The difference

$$\Delta p_t(n) = n < p_t^2 > - < (\sum_{i=1}^{n} \vec{p}_{t_i})^2 > \tag{4.8}$$

provides a simple measure of the degree of transverse momentum correlation. Fig. 11a shows this quantity for M^+p interactions as a function of n. The data are restricted to charged particles in the interval $0< y <1$ where the influence of momentum conservation and of cascading should be small. The fact that $\Delta p_t(n)$ is positive and increasing with n, reflects local transverse momentum correlations as

[4]For example, in the multi-string dual Parton Model the strength of the two-particle rapidity correlation is inversely proportional to the number of strings

expected. This is supported by the agreement of the data with the DPM prediction (dashed curve) where such correlations are explicitly built-in.

Fig. 11b compares the results for nuclear collisions with the smoothed M^+p data of Fig. 11a (solid curve). Although the errors are too large to draw strong conclusions, there is a tendency of the nuclear data to fall below those for M^+p. An intuitive explanation can be offered: in nuclear interactions, particles are produced in several collisions, which helps to randomize the $\vec{p}_t$ vectors.

5 Stopping Power

The amount of energy lost by a projectile or a "leading" projectile fragment, as a result of multiple collisions in nuclear matter is commonly called the nuclear "stopping power" [11]. It is natural to expect that some characteristics of hadron production, in particluar the number of produced hadrons, is correlated with this energy loss. Although conceptually well-defined, the stopping power is difficult to estimate experimentally. Following the suggestions in [12], we adopt as the measure of the stopping power the variable $\Delta y_{max} = y_{max} - y_{beam}$ where y_{max} is the largest rapidity value of all the charged particles in an event[5] and y_{beam} is the rapidity of the beam particle.

Fig. 12 shows the normalized distribution $\varrho(\Delta y_{max})$ for M^+p, M^+Al and M^+Au collisions[6]. As expected, the distribution shifts to larger (negative) values of Δy_{max} as A increases. The average multiplicity of negative particles as a function of Δy_{max} is presented in Fig. 13 and compared to the DPM predictions. The model reproduces only qualitatively the shape and the strong A-dependence of the data. The disagreement at large negative values of Δy_{max} is expected since the model neglects nuclear cascading. Note however that the DPM is unable to describe the data even for elementary M^+p collisions.

In the framework of the Additive Quark Model, the distribution $\varrho_A(\Delta y_{max})$ can be written as

$$\varrho_A(\Delta y_{max}) = P_s F_1(\Delta y_{max}) + (1 - P_s) F_2(\Delta y_{max}), \tag{5.9}$$

where $F_1(\Delta y_{max})$ and $F_2(\Delta y_{max})$ are the normalized fragmentation functions, resulting from the wounding of a single quark (as e.g. in an elementary collision) and the wounding of two quarks (in the collision with a nucleus). P_s is the calculable probability that a single quark was a spectator ($P_s = P_{s_q} + P_{s_{\bar{q}}}$ from subsect. 3.3). Taking the functional form of $F_1(\Delta y_{max})$ from K^+p and π^+p interactions, one can

[5] In most cases this is a positive particle, but in general a "fragment" of a "projectile" needs not necessarily to carry the same charge.

[6] The shape of the distribution of Δy_{max} differs from the proton beam data of Toothacker et al. [13] because these authors used only identified fast protons to calculate the rapidity difference w.r.t. the projectile and they did not eliminate elastic and coherent events.

derive $F_2(\Delta y_{max})$ for both beam types and targets independently. The results are shown in Figs. 14a and 14b. The fragmentation function $F_2(\Delta y_{max})$ is practically the same for Al and Au targets and also very similar for both projectiles (π^+ and K^+).

Interactions with a large number of grey protons presumably have larger than average probability to originate from the wounding of the two valence quarks in the projectile. As an additional check of the AQM picture, we therefore determined $\varrho(\Delta y_{max})$ for $\pi^+ Au$ interactions with $n_g > 6$. If the probabilities P_{sq} and $P_{s\overline{q}}$ are small, $\rho(\Delta y_{max})$ is expected to coincide with $F_2(\Delta y_{max})$ (Fig. 14b). The comparison of both functions in Fig. 15 shows that this is indeed the case[7].

Finally we show in Fig. 16 the average value of the variable

$$z = \frac{E_{particle}}{E_{beam}}$$

for the three reactions studied, as a function of the particle ordering in rapidity, particle 1 having the largest rapidity, 2 the second largest, etc. From this figure it is clear that the average energy of the "fastest" particle strongly depends on the atomic mass number, whereas $< z >$ of the second and further particles is nearly A-independent. This observation lends support to the use of the fastest particle, and therefore of the variable Δy_{max}, as a measure of the stopping power of the nucleus: the difference in $< z >$ between proton, Al and Au targets is only seen for the fastest particle.

6 Summary and conclusions

We have analysed the rapidity, transverse momentum and event maximal rapidity distributions in interactions of π^+ and K^+ mesons of 250 GeV/c with aluminum and gold nuclei. The data have been collected with the EHS detector at the CERN SPS.

Earlier findings are confirmed by our observations. New results have been presented, in particular on K^+ interactions on nuclei at the highest available beam momentum. The main results can be summarized as follows.

- The rapidity distributions in interactions with a nucleus can be described as a sum of contributions from a first interaction of the incident particle with one of the nucleons, which is alike an elementary interaction on protons, followed by a number of lower energy secondary interactions, each with similar rapidity distribution.

[7]According to the AQM calculation one finds that $P_{ww} \approx 0.85$ for $n_g > 6$ ($\overline{\nu} = 4.8$). The small contribution from $P_s F_1(\Delta y_{max})$ to $\varrho(\Delta y_{max})$ in (5.9) is therefore neglected in Fig. 15.

- Transverse momentum distributions are quite different in nuclear and elementary collisions. The comparison of the two reveals an excess of large p_t ($p_t > 1.$ GeV/c) particles in nuclear collisions.
- Also the dependence of the average transverse momentum on charge multiplicity and Feynman x_F of negative particles is different in elementary and in nuclear collisions.

The results presented here are consistent with the concept of multiple collisions inside the nucleus. Comparison of our data with the AQM and DPM leads to the following conclusions.

The Dual Parton Model:

- reproduces reasonably well the ratio $R(y)$ in the central and projectile fragmentation regions;
- obviously fails in the target fragmentation region since the process of cascading is explicitly ignored in the model used;
- does not describe the event maximal rapidity distributions (which can be considered as a measure of the nuclear stopping power) for nuclear and, surprisingly, also for elementary collisions.

The Additive Quark Model:

- gives a consistent parametrization of the rapidity distribution in terms of the spectator and wounded quark fragmentation functions in the forward hemisphere;
- helps to parametrize conveniently the event maximal rapidity distribution in terms of one and two wounded quarks fragmentation functions;
- is consistent with the global behavior of the rapidity distributions in the central region.

Acknowledgments

We are indebted to the CERN SPS, beam and EHS crews for their support during the run of our experiment. It is a pleasure to thank the scanning and measuring staffs of our laboratories. The contribution of the Aachen group to the earlier phase of this experiment is gratefully acknowledged.

7 References

1. A. Capella et al.: Proc. XVII Inter. Symp. on Multipart. Dynamics 1986, ed. M.Markytan, W.Majerotto and J.MacNaughton, (World Scientific, Singapore, 1987), 781

2. A. Białas, W. Czyż, W. Furmański: Acta Phys. Pol. **B8** (1977) 585
   A. Białas, E. Białas: Phys. Rev. **D20** (1978) 3357

3. S. Fredriksson, G. Eilam, G. Berlad, L. Bergström: Phys. Rep. **144** (1987) 188

4. I.V. Ajinenko et al. (NA22 Coll.): Z. Phys. C - Particles and Fields **42** (1989) 377

5. I.V. Ajinenko et al. (NA22 Coll.): Z. Phys. C - Particles and Fields **46** (1990) 569

6. K. Fiałkowski: Acta Phys. Pol. **B17** (1986) 623

   R. Hołynski: *"Hadron interactions in emulsions in the energy interval 60 to 400 GeV*, IFJ Rapport No 1303/PH (in Polish)

7. B. Andersson, I. Otterlund, E. Stenlund: Phys. Lett. **73B** (1978) 343

8. R. Hołynski, M. Jeżabek, K. Woźniak: Z. Phys. C - Particles and Fields **31** (1986) 467

9. D.H. Brick et al.: Phys. Rev. **D41** (1990) 765

10. M. Adamus et al. (NA22 Coll.): Z. Phys. C - Particles and Fields **39** (1988) 311

11. For a review, see W. Busza, P. Ledoux: Ann. Rev. Nucl. and Part. Sciences **38** (1988) 119

12. W. Busza, A.S. Goldhaber: Phys. Lett. **B139** (1987) 235
    S. Date et al.: Phys. Rev. **D32** (1985) 619
    M. Jeżabek et al.: Z. Phys. C - Particles and Fields **29** (1986) 55

13. W.S. Toothacker et al.: Phys. Lett. **B197** (1987) 295

Table 1a. Rapidity density of charged particles $\varrho_A(y)$ for $\pi^+ Al$ interactions at 250 GeV/c. In the third column protons with $p_{lab} < 1.2$ GeV/c are excluded.

$y - interval$	$(1/N_{ev})(dN/dy)$		
	all positives	*positives (protons excluded)*	*all negatives*
$-5.5 \div (-5.0)$	0.001 ± 0.001	0.001 ± 0.001	$- - - -$
$-5.0 \div (-4.5)$	0.005 ± 0.002	0.005 ± 0.002	0.003 ± 0.001
$-4.5 \div (-4.0)$	0.043 ± 0.005	0.043 ± 0.005	0.012 ± 0.003
$-4.0 \div (-3.5)$	0.181 ± 0.011	0.146 ± 0.010	0.084 ± 0.007
$-3.5 \div (-3.0)$	1.183 ± 0.028	0.326 ± 0.015	0.218 ± 0.012
$-3.0 \div (-2.5)$	1.927 ± 0.036	0.667 ± 0.021	0.420 ± 0.017
$-2.5 \div (-2.0)$	1.152 ± 0.028	0.942 ± 0.025	0.683 ± 0.022
$-2.0 \div (-1.5)$	1.208 ± 0.028	1.208 ± 0.028	0.870 ± 0.024
$-1.5 \div (-1.0)$	1.415 ± 0.031	1.415 ± 0.031	1.047 ± 0.026
$-1.0 \div (-0.5)$	1.417 ± 0.030	1.417 ± 0.030	1.129 ± 0.027
$-0.5 \div 0.0$	1.414 ± 0.030	1.414 ± 0.030	1.147 ± 0.027
$0.0 \div 0.5$	1.378 ± 0.030	1.378 ± 0.030	1.112 ± 0.027
$0.5 \div 1.0$	1.286 ± 0.029	1.286 ± 0.029	1.109 ± 0.027
$1.0 \div 1.5$	1.196 ± 0.028	1.196 ± 0.028	0.805 ± 0.023
$1.5 \div 2.0$	0.938 ± 0.024	0.938 ± 0.024	0.641 ± 0.020
$2.0 \div 2.5$	0.685 ± 0.021	0.685 ± 0.021	0.461 ± 0.017
$2.5 \div 3.0$	0.400 ± 0.016	0.400 ± 0.016	0.222 ± 0.012
$3.0 \div 3.5$	0.193 ± 0.011	0.193 ± 0.011	0.086 ± 0.007
$3.5 \div 4.0$	0.114 ± 0.008	0.114 ± 0.008	0.024 ± 0.004
$4.0 \div 4.5$	0.045 ± 0.006	0.045 ± 0.006	0.008 ± 0.002
$4.5 \div 5.0$	0.017 ± 0.006	0.017 ± 0.006	0.002 ± 0.001

Table 1b. Rapidity density of charged particles $\varrho_A(y)$ for K^+Al interactions at 250 GeV/c

$y-interval$	$(1/N_{ev})(dN/dy)$		
	all positives	*positives (protons excluded)*	*all negatives*
$-5.5 \div (-5.0)$	– – – –	– – – –	– – – –
$-5.0 \div (-4.5)$	– – – –	– – – –	– – – –
$-4.5 \div (-4.0)$	0.046 ± 0.009	0.046 ± 0.009	0.009 ± 0.004
$-4.0 \div (-3.5)$	0.184 ± 0.019	0.141 ± 0.017	0.077 ± 0.013
$-3.5 \div (-3.0)$	1.212 ± 0.049	0.353 ± 0.026	0.236 ± 0.022
$-3.0 \div (-2.5)$	1.986 ± 0.062	0.644 ± 0.035	0.450 ± 0.029
$-2.5 \div (-2.0)$	1.138 ± 0.047	0.899 ± 0.042	0.618 ± 0.035
$-2.0 \div (-1.5)$	1.197 ± 0.048	1.194 ± 0.048	0.927 ± 0.043
$-1.5 \div (-1.0)$	1.417 ± 0.053	1.417 ± 0.053	0.955 ± 0.043
$-1.0 \div (-0.5)$	1.470 ± 0.053	1.470 ± 0.053	1.166 ± 0.048
$-0.5 \div 0.0$	1.373 ± 0.051	1.373 ± 0.051	1.157 ± 0.047
$0.0 \div 0.5$	1.486 ± 0.053	1.486 ± 0.053	1.166 ± 0.047
$0.5 \div 1.0$	1.309 ± 0.050	1.309 ± 0.050	1.113 ± 0.046
$1.0 \div 1.5$	1.110 ± 0.046	1.110 ± 0.046	0.844 ± 0.040
$1.5 \div 2.0$	0.873 ± 0.040	0.873 ± 0.040	0.601 ± 0.034
$2.0 \div 2.5$	0.636 ± 0.034	0.636 ± 0.034	0.416 ± 0.028
$2.5 \div 3.0$	0.438 ± 0.028	0.438 ± 0.028	0.171 ± 0.018
$3.0 \div 3.5$	0.196 ± 0.019	0.196 ± 0.019	0.086 ± 0.013
$3.5 \div 4.0$	0.073 ± 0.012	0.073 ± 0.012	0.025 ± 0.007
$4.0 \div 4.5$	0.040 ± 0.010	0.040 ± 0.010	0.004 ± 0.003
$4.5 \div 5.0$	0.009 ± 0.004	0.009 ± 0.004	

Table 1c. Rapidity density of charged particles $\varrho_A(y)$ for $\pi^+ Au$ interactions at 250 GeV/c

$y-interval$	$(1/N_{ev})(dN/dy)$		
	all positives	*positives (protons excluded)*	*all negatives*
$-5.5 \div (-5.0)$	0.003 ± 0.002	0.003 ± 0.002	$- - - -$
$-5.0 \div (-4.5)$	0.026 ± 0.005	0.026 ± 0.005	0.002 ± 0.001
$-4.5 \div (-4.0)$	0.146 ± 0.011	0.146 ± 0.011	0.025 ± 0.005
$-4.0 \div (-3.5)$	0.500 ± 0.021	0.372 ± 0.018	0.159 ± 0.012
$-3.5 \div (-3.0)$	3.778 ± 0.057	0.861 ± 0.027	0.516 ± 0.021
$-3.0 \div (-2.5)$	5.100 ± 0.066	1.631 ± 0.038	0.940 ± 0.028
$-2.5 \div (-2.0)$	2.321 ± 0.045	1.876 ± 0.040	1.212 ± 0.032
$-2.0 \div (-1.5)$	2.070 ± 0.042	2.070 ± 0.042	1.494 ± 0.035
$-1.5 \div (-1.0)$	2.083 ± 0.042	2.083 ± 0.042	1.473 ± 0.035
$-1.0 \div (-0.5)$	1.947 ± 0.040	1.947 ± 0.040	1.410 ± 0.034
$-0.5 \div 0.0$	1.794 ± 0.038	1.794 ± 0.038	1.463 ± 0.034
$0.0 \div 0.5$	1.607 ± 0.036	1.607 ± 0.036	1.310 ± 0.032
$0.5 \div 1.0$	1.411 ± 0.033	1.411 ± 0.033	1.173 ± 0.030
$1.0 \div 1.5$	1.242 ± 0.031	1.242 ± 0.031	0.977 ± 0.027
$1.5 \div 2.0$	0.990 ± 0.027	0.990 ± 0.027	0.687 ± 0.023
$2.0 \div 2.5$	0.649 ± 0.022	0.649 ± 0.022	0.415 ± 0.017
$2.5 \div 3.0$	0.357 ± 0.016	0.357 ± 0.016	0.214 ± 0.012
$3.0 \div 3.5$	0.181 ± 0.011	0.181 ± 0.011	0.072 ± 0.007
$3.5 \div 4.0$	0.102 ± 0.009	0.102 ± 0.009	0.017 ± 0.003
$4.0 \div 4.5$	0.023 ± 0.040	0.023 ± 0.040	0.004 ± 0.002
$4.5 \div 5.0$	0.006 ± 0.002	0.006 ± 0.002	0.001 ± 0.001

Table 1d. Rapidity density $\varrho_A(y)$ of charged particles for K^+Au interactions at 250 GeV/c

$y-interval$	$(1/N_{ev})(dN/dy)$		
	all positives	*positives (protons excluded)*	*all negatives*
$-5.5 \div (-5.0)$	0.005 ± 0.004	0.005 ± 0.004	$- - - -$
$-5.0 \div (-4.5)$	0.019 ± 0.007	0.019 ± 0.007	$- - - -$
$-4.5 \div (-4.0)$	0.129 ± 0.018	0.129 ± 0.018	0.020 ± 0.007
$-4.0 \div (-3.5)$	0.508 ± 0.035	0.379 ± 0.031	0.172 ± 0.020
$-3.5 \div (-3.0)$	4.166 ± 0.101	0.835 ± 0.046	0.525 ± 0.036
$-3.0 \div (-2.5)$	5.248 ± 0.114	1.485 ± 0.061	0.934 ± 0.049
$-2.5 \div (-2.0)$	2.283 ± 0.074	1.749 ± 0.065	1.233 ± 0.054
$-2.0 \div (-1.5)$	2.180 ± 0.073	2.178 ± 0.073	1.475 ± 0.059
$-1.5 \div (-1.0)$	2.115 ± 0.070	2.115 ± 0.070	1.423 ± 0.058
$-1.0 \div (-0.5)$	1.954 ± 0.068	1.954 ± 0.068	1.469 ± 0.058
$-0.5 \div 0.0$	1.777 ± 0.063	1.777 ± 0.063	1.359 ± 0.055
$0.0 \div 0.5$	1.566 ± 0.059	1.566 ± 0.059	1.350 ± 0.055
$0.5 \div 1.0$	1.328 ± 0.055	1.328 ± 0.055	1.193 ± 0.052
$1.0 \div 1.5$	1.244 ± 0.052	1.244 ± 0.052	0.968 ± 0.046
$1.5 \div 2.0$	1.022 ± 0.047	1.022 ± 0.047	0.693 ± 0.038
$2.0 \div 2.5$	0.626 ± 0.036	0.626 ± 0.036	0.365 ± 0.027
$2.5 \div 3.0$	0.350 ± 0.027	0.350 ± 0.027	0.170 ± 0.019
$3.0 \div 3.5$	0.210 ± 0.021	0.210 ± 0.021	0.051 ± 0.010
$3.5 \div 4.0$	0.070 ± 0.012	0.070 ± 0.012	0.016 ± 0.006
$4.0 \div 4.5$	0.041 ± 0.012	0.041 ± 0.012	$- - - -$
$4.5 \div 5.0$	0.005 ± 0.003	0.005 ± 0.003	$- - - -$

Table 2. Definition of subsamples used in the analysis:
$\overline{\nu}$ is the average number of collisions, calculated from the Andersson model [7],
$P_{\overline{\nu}}$ the probability of $\overline{\nu}$ collisions

			$\overline{\nu}$	$P_{\overline{\nu}}$
π^+	Al	$n_g = 0$	1.36	0.418
		$n_g = 1$	1.71	0.268
		$n_g = 2$	2.09	0.150
		$n_g = 3$	2.46	0.080
		$n_g \geq 4$	3.12	0.084
	Au	$n_g = 0$	1.69	0.273
		$n_g = 1$	2.34	0.162
		$n_g = 2$	2.78	0.121
		$n_g = 3$	3.14	0.095
		$n_g = 4$	3.44	0.075
		$n_g = 5, 6$	3.81	0.107
		$n_g \geq 7$	4.70	0.167
K^+	Al	$n_g = 0$	1.31	0.429
		$n_g = 1$	1.61	0.270
		$n_g = 2$	1.93	0.147
		$n_g = 3$	1.25	0.077
		$n_g \geq 4$	2.83	0.077
	Au	$n_g = 0$	1.59	0.296
		$n_g = 1$	2.12	0.159
		$n_g = 2$	2.48	0.117
		$n_g = 3$	2.78	0.091
		$n_g = 4$	3.02	0.070
		$n_g = 5, 6$	3.33	0.102
		$n_g \geq 7$	4.09	0.165

Table 3a. Normalized transverse momentum distributions $g_A(p_t)$ for π^+Al and π^+Au interactions at 250 GeV/c

$p_t - interval$ (GeV/c)	$(1/N)(dN/dp_t)(GeV/c)^{-1}$			
	Al		*Au*	
	positives	*negatives*	*positives*	*negatives*
0.00 ÷ 0.05	0.458 ± 0.021	0.572 ± 0.049	0.334 ± 0.023	0.467 ± 0.049
0.05 ÷ 0.10	1.172 ± 0.031	1.408 ± 0.060	1.067 ± 0.031	1.329 ± 0.060
0.10 ÷ 0.15	1.688 ± 0.037	1.892 ± 0.070	1.614 ± 0.035	2.046 ± 0.070
0.15 ÷ 0.20	1.890 ± 0.039	2.164 ± 0.070	1.973 ± 0.037	2.240 ± 0.070
0.20 ÷ 0.25	1.998 ± 0.040	2.122 ± 0.067	1.919 ± 0.036	2.127 ± 0.067
0.25 ÷ 0.30	1.848 ± 0.039	1.949 ± 0.063	1.783 ± 0.035	1.938 ± 0.063
0.30 ÷ 0.35	1.673 ± 0.037	1.658 ± 0.060	1.733 ± 0.034	1.746 ± 0.060
0.35 ÷ 0.40	1.439 ± 0.034	1.395 ± 0.055	1.568 ± 0.032	1.471 ± 0.055
0.40 ÷ 0.45	1.291 ± 0.032	1.279 ± 0.050	1.338 ± 0.030	1.226 ± 0.050
0.45 ÷ 0.50	1.132 ± 0.030	1.007 ± 0.045	1.131 ± 0.028	1.040 ± 0.045
0.50 ÷ 0.55	0.908 ± 0.027	0.805 ± 0.040	0.905 ± 0.025	0.808 ± 0.040
0.55 ÷ 0.60	0.795 ± 0.025	0.705 ± 0.038	0.768 ± 0.023	0.715 ± 0.038
0.60 ÷ 0.65	0.662 ± 0.023	0.530 ± 0.033	0.618 ± 0.020	0.558 ± 0.033
0.65 ÷ 0.70	0.519 ± 0.020	0.479 ± 0.030	0.499 ± 0.018	0.471 ± 0.030
0.70 ÷ 0.75	0.441 ± 0.019	0.359 ± 0.026	0.460 ± 0.018	0.359 ± 0.026
0.75 ÷ 0.80	0.333 ± 0.016	0.291 ± 0.023	0.344 ± 0.015	0.279 ± 0.023
0.80 ÷ 0.85	0.292 ± 0.015	0.235 ± 0.021	0.285 ± 0.014	0.235 ± 0.017
0.85 ÷ 0.90	0.236 ± 0.014	0.212 ± 0.019	0.246 ± 0.013	0.195 ± 0.019
0.90 ÷ 0.95	0.216 ± 0.013	0.165 ± 0.018	0.218 ± 0.012	0.178 ± 0.018
0.95 ÷ 1.00	0.154 ± 0.011	0.154 ± 0.017	0.168 ± 0.011	0.141 ± 0.017
1.00 ÷ 1.05	0.119 ± 0.010	0.093 ± 0.016	0.145 ± 0.010	0.123 ± 0.016
1.05 ÷ 1.15	0.102 ± 0.006	0.079 ± 0.009	0.101 ± 0.011	0.092 ± 0.009
1.15 ÷ 1.25	0.066 ± 0.005	0.051 ± 0.008	0.077 ± 0.005	0.060 ± 0.008
1.25 ÷ 1.35	0.047 ± 0.004	0.035 ± 0.007	0.046 ± 0.004	0.046 ± 0.007
1.35 ÷ 1.45	0.038 ± 0.004	0.026 ± 0.006	0.034 ± 0.003	0.033 ± 0.006
1.45 ÷ 1.55	0.028 ± 0.003	0.021 ± 0.004	0.026 ± 0.003	0.016 ± 0.004
1.55 ÷ 1.75	0.014 ± 0.002	0.013 ± 0.002	0.013 ± 0.002	0.012 ± 0.002
1.75 ÷ 1.95	0.007 ± 0.001	0.009 ± 0.002	0.007 ± 0.001	0.011 ± 0.002
1.95 ÷ 2.35	0.005 ± 0.001	0.003 ± 0.001	0.005 ± 0.001	0.005 ± 0.001
2.35 ÷ 2.75	0.002 ± 0.001	0.002 ± 0.001	0.003 ± 0.001	0.002 ± 0.001
2.75 ÷ 3.15	0.001 ± 0.001	0.001 ± 0.001	0.002 ± 0.001	0.001 ± 0.001

Table 3b. Normalized transverse momentum distributions $g_A(p_t)$ for K^+Al and K^+Au interactions at 250 GeV/c

$p_t - interval$ (GeV/c)	$(1/N)(dN/dp_t)(GeV/c)^{-1}$			
	Al		Au	
	positives	*negatives*	*positives*	*negatives*
$0.00 \div 0.05$	0.462 ± 0.037	0.602 ± 0.081	0.333 ± 0.038	0.437 ± 0.081
$0.05 \div 0.10$	1.177 ± 0.054	1.344 ± 0.108	0.989 ± 0.049	1.475 ± 0.108
$0.10 \div 0.15$	1.656 ± 0.064	2.057 ± 0.119	1.714 ± 0.058	2.148 ± 0.119
$0.15 \div 0.20$	1.906 ± 0.068	2.228 ± 0.122	2.021 ± 0.063	2.445 ± 0.122
$0.20 \div 0.25$	1.827 ± 0.066	2.229 ± 0.112	1.889 ± 0.060	2.096 ± 0.112
$0.25 \div 0.30$	1.882 ± 0.068	1.934 ± 0.109	1.875 ± 0.060	2.025 ± 0.109
$0.30 \div 0.35$	1.695 ± 0.064	1.674 ± 0.103	1.721 ± 0.057	1.817 ± 0.103
$0.35 \div 0.40$	1.531 ± 0.061	1.405 ± 0.088	1.448 ± 0.052	1.353 ± 0.088
$0.40 \div 0.45$	1.212 ± 0.054	1.321 ± 0.083	1.362 ± 0.051	1.212 ± 0.083
$0.45 \div 0.50$	1.101 ± 0.052	0.961 ± 0.078	1.075 ± 0.045	1.060 ± 0.078
$0.50 \div 0.55$	0.978 ± 0.048	0.709 ± 0.064	0.838 ± 0.040	0.733 ± 0.064
$0.55 \div 0.60$	0.752 ± 0.043	0.636 ± 0.058	0.797 ± 0.039	0.613 ± 0.058
$0.60 \div 0.65$	0.624 ± 0.039	0.551 ± 0.053	0.647 ± 0.035	0.492 ± 0.053
$0.65 \div 0.70$	0.489 ± 0.034	0.471 ± 0.050	0.532 ± 0.032	0.430 ± 0.050
$0.70 \div 0.75$	0.429 ± 0.032	0.319 ± 0.045	0.418 ± 0.028	0.364 ± 0.045
$0.75 \div 0.80$	0.401 ± 0.031	0.320 ± 0.037	0.398 ± 0.027	0.232 ± 0.037
$0.80 \div 0.85$	0.289 ± 0.026	0.256 ± 0.037	0.335 ± 0.025	0.255 ± 0.037
$0.85 \div 0.90$	0.252 ± 0.024	0.159 ± 0.030	0.289 ± 0.023	0.171 ± 0.030
$0.90 \div 0.95$	0.202 ± 0.022	0.123 ± 0.029	0.194 ± 0.020	0.146 ± 0.029
$0.95 \div 1.00$	0.182 ± 0.021	0.088 ± 0.034	0.178 ± 0.018	0.148 ± 0.034
$1.00 \div 1.05$	0.168 ± 0.020	0.104 ± 0.030	0.151 ± 0.017	0.146 ± 0.030
$1.05 \div 1.15$	0.098 ± 0.011	0.073 ± 0.014	0.102 ± 0.010	0.062 ± 0.014
$1.15 \div 1.25$	0.083 ± 0.010	0.048 ± 0.011	0.080 ± 0.009	0.049 ± 0.011
$1.25 \div 1.35$	0.060 ± 0.008	0.028 ± 0.011	0.038 ± 0.006	0.042 ± 0.011
$1.35 \div 1.45$	0.039 ± 0.007	0.027 ± 0.009	0.040 ± 0.006	0.026 ± 0.009
$1.45 \div 1.55$	0.021 ± 0.005	0.017 ± 0.007	0.027 ± 0.005	0.019 ± 0.007
$1.55 \div 1.75$	0.013 ± 0.003	0.013 ± 0.005	0.015 ± 0.003	0.016 ± 0.005
$1.75 \div 1.95$	0.008 ± 0.002	0.002 ± 0.002	0.010 ± 0.002	0.002 ± 0.002
$1.95 \div 2.35$	0.007 ± 0.001	0.002 ± 0.002	0.005 ± 0.001	0.004 ± 0.002
$2.35 \div 2.75$	0.002 ± 0.001	0.002 ± 0.001	0.002 ± 0.001	0.003 ± 0.001
$2.75 \div 3.15$	0.001 ± 0.001	0.002 ± 0.001	0.001 ± 0.001	0.002 ± 0.001

Table 3c. Correction factors used in order to take into account the contribution from unidentified electrons and positrons. All factors are equal to one for $p_t > 0.80$ GeV/c.

$p_t - interval$ (GeV/c)	Correction factors			
	Al		*Au*	
	positives	*negatives*	*positives*	*negatives*
$0.00 \div 0.05$	0.807	0.771	0.428	0.382
$0.05 \div 0.10$	0.955	0.954	0.766	0.718
$0.10 \div 0.15$	0.981	0.981	0.885	0.867
$0.15 \div 0.20$	0.992	0.992	0.944	0.930
$0.20 \div 0.25$	0.993	0.993	0.962	0.952
$0.25 \div 0.30$	0.994	0.994	0.974	0.966
$0.30 \div 0.35$	0.996	0.996	0.981	0.971
$0.35 \div 0.40$	0.999	0.999	0.988	0.981
$0.40 \div 0.45$	0.999	0.999	0.991	0.983
$0.45 \div 0.50$	0.999	0.999	0.989	0.988
$0.50 \div 0.55$	1.000	1.000	0.994	0.988
$0.55 \div 0.60$	1.000	1.000	0.993	0.989
$0.60 \div 0.65$	1.000	1.000	0.996	0.991
$0.65 \div 0.70$	1.000	1.000	0.998	0.993
$0.70 \div 0.75$	1.000	1.000	1.000	0.999
$0.75 \div 0.80$	1.000	1.000	1.000	1.000

Figure Captions

Fig. 1 a–b Rapidity density $\varrho(y)$ for K^+Al and K^+Au interactions: **a** positive particles, **b** negative particles. The curves join the experimental points to guide the eye. Open symbols: data after exclusion of identified protons.

Fig. 2 Fitted functions $a(y)$ and $b(y)$ for negative particles (the samples of π^+ and K^+ interactions are merged - M^+ stands for π^+ or K^+)

Fig. 3 a–b a Comparison of $a(y)$ with the rapidity density $\varrho_p(y)$ for negative particles in elementary M^+p collisions (solid line) and with the DPM prediction (dashed curve).
b Comparison of $b(y)$ with the DPM prediction (dashed curve). The experimental data points for M^+Al are marked with full triangles and for M^+Au with full circles.

Fig. 4 a–b Ratio $R(y) = \varrho_A(y)/\varrho_p(y)$ **a)** for positive particles (protons included), **b)** for negative particles. Open symbols: K^+ beam, full symbols: π^+ beam. Solid (dashed) curves are predictions of the DPM for the Au (Al) target.

Fig. 5 a–d Ratio $R^-(y) = \varrho_A(y)/\varrho_p(y)$ for negative particles in different rapidity regions:
a vs $\overline{\nu}$ for $y < -2.5$, **b** vs n_g for $y < -2.5$, **c** vs $\overline{\nu}$ for $-0.5 < y < 1.0$ and **d** vs $\overline{\nu}$ for $y > 2.5$. In **c** the arrows indicate the limiting values for the AQM. The dashed line is the DPM prediction.

Fig. 6 a–b Fragmentation functions F_w of wounded and F_s of spectator quarks, fitted with formula (3.4) taken from the AQM. **a** positive particles, protons included, **b** negative particles.

Fig. 7 a–b Comparison of the rapidity density $\varrho_p(y)$ for elementary M^+p collisions (crosses) with the expectation of the AQM (see formula 3.5 in the text). **a** positive particles, protons included, **b** negative particles. The curves join the experimental points to guide the eye.

Fig. 8 a–c Average transverse momentum $< p_t >$ of negative particles as a function of the negative particle multiplicity n^- (π^+ and K^+ beam samples are merged).

Fig. 9 a–d Ratio $R(p_t) = g_A(p_t)/g_p(p_t)$ for the M^+ sample: **a** positive particles, protons included, from M^+Al, **b** positive particles, protons included, from M^+Au, **c** negative particles from M^+Al and **d** negative particles from M^+Au.

Fig. 9 e–h Ratio $R(p_t) = g_A(p_t)/g_p(p_t)$ for negative particles in the M^+ sample: **e** $y > 0$ in M^+Al, **f** $y > 0$ in M^+Au, **g** $y < 0$ in M^+Al and **h** $y < 0$ in M^+Au,

Fig. 10 Average transverse momentum $< p_t >$ of negative particles as a function of Feynman x_F (π^+ and K^+ beam samples combined). M^+p: the curve, M^+Al: triangles, M^+Au: circles.

Fig. 11 a–b The value of the difference: $n < p_t^2 > - < (\Sigma_n \vec{p_t^2}) >$ as a function of charge multiplicity n in the rapidity region $0. < y < 1.$ for the M^+ sample. **a** comparison of elementary collision data M^+p with the DPM prediction (dashed curve). **b** M^+Au: circles, M^+Al: triangles, M^+p: full curve.

Fig. 12 Density distribution of the difference Δy_{max} (difference between the maximal rapidity of the charged particles in an event and the rapidity of the beam particle) for the M^+p, M^+Al and M^+Au collisions. The curves connecting the data points are drawn to guide the eye.

Fig. 13 The average number of negative particles as a function of Δy_{max} for M^+p, M^+Al and M^+Au collisions. DPM predictions as indicated.

Fig. 14 a–b The AQM fragmentation function F_2 as a function of Δy_{max} obtained from the fit of formula (5.9) to the data. **a** for the K^+ beam and **b** for the π^+ beam. The curves are to guide the eye (for nuclear targets the curve is drawn through the average between Au and Al points).

Fig. 15 Density distribution of Δy_{max} for the highly inelastic sample of π^+Au collisions with number of grey protons $n_g > 6$. The full curve represents $F_2(\Delta y_{max})$

Fig. 16 Average fraction of the incident energy carried by the fastest, second fastest, ... particle for the three reactions studied.

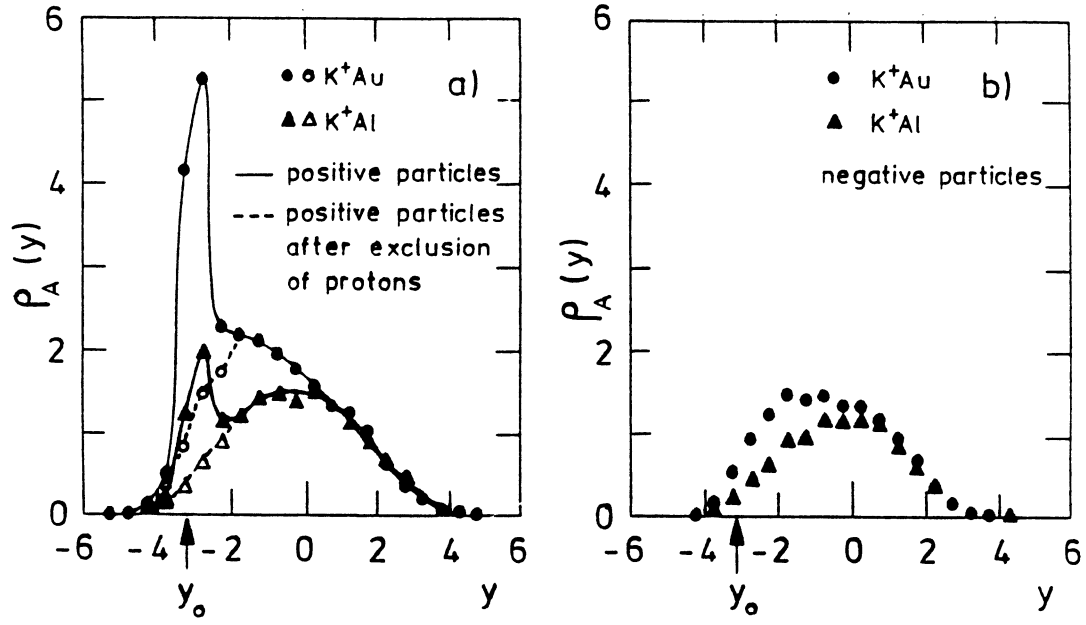
a)
b)
K+Au
K+Al
positive particles
positive particles after exclusion of protons
negative particles
ρA (y)
y
y0

Fig. 1

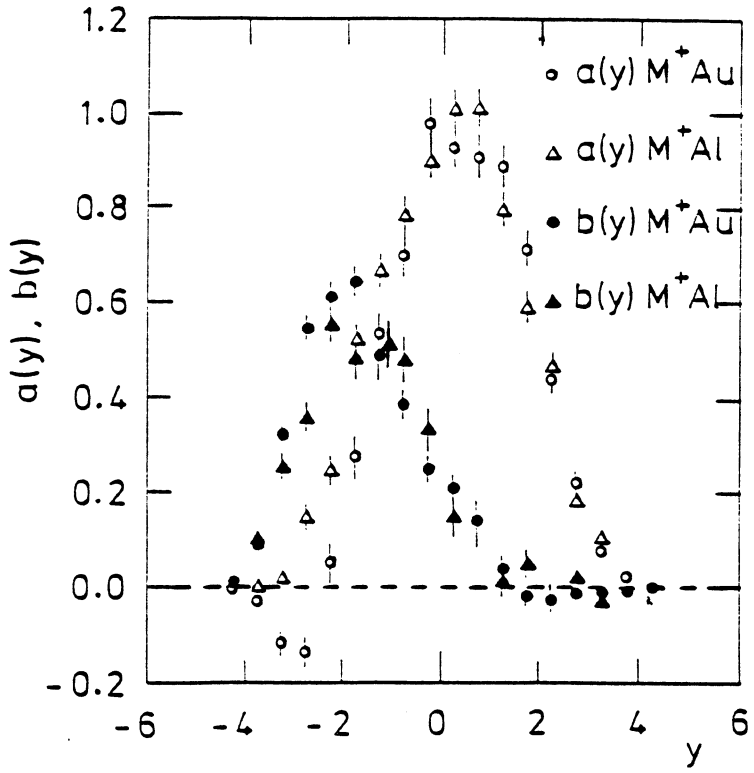
a(y) M+Au
a(y) M+Al
b(y) M+Au
b(y) M+Al
a(y), b(y)
y

Fig. 2

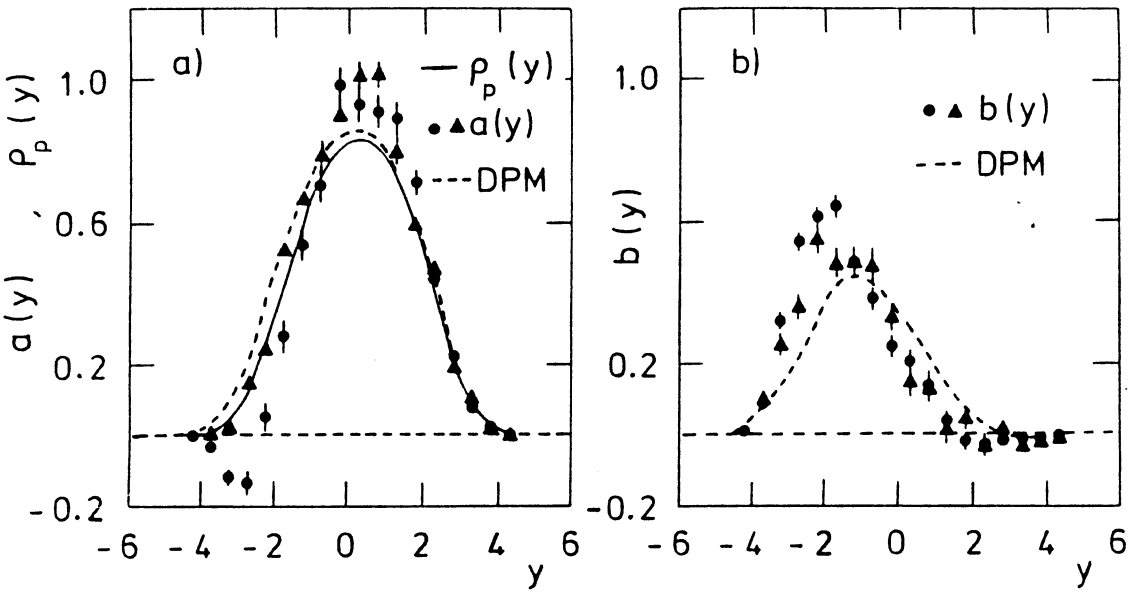
a)
ρ_p (y)
a(y)
---DPM
ρ_p (y)
a(y)
1.0
0.6
0.2
-0.2
-6 -4 -2 0 2 4 6
y
b)
b(y)
--- DPM
b(y)
1.0
0.2
-0.2
-6 -4 -2 0 2 4 6
y

Fig. 3

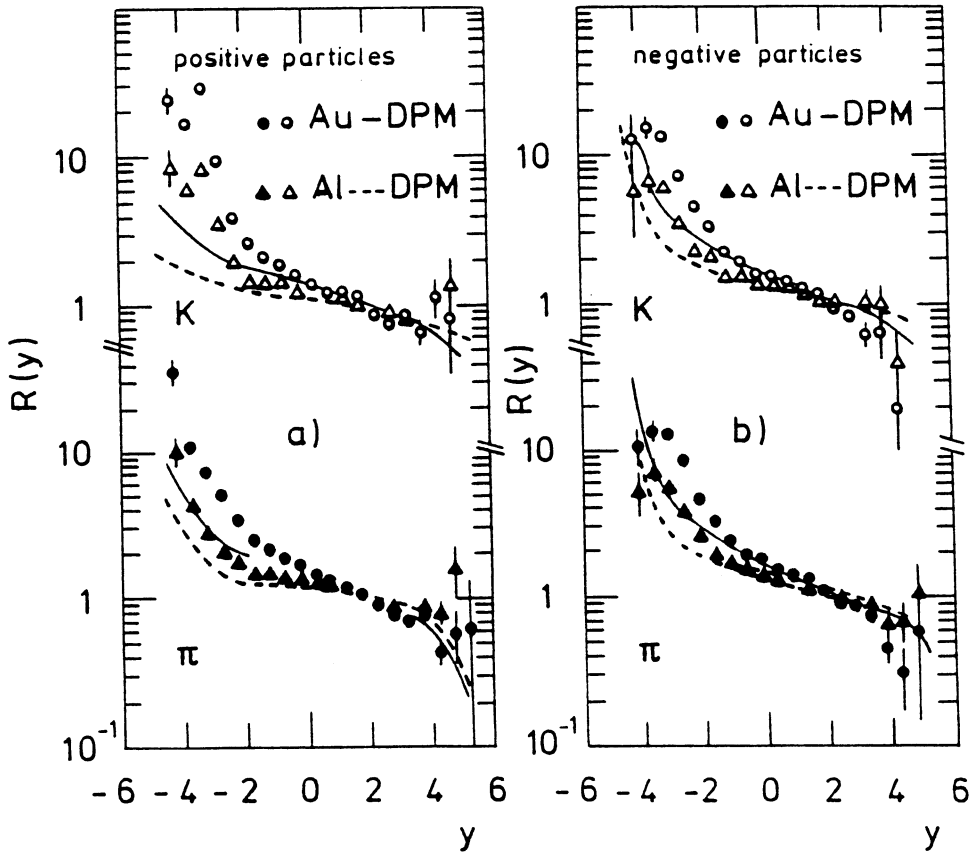
positive particles
Au – DPM
Al---DPM
K
a)
π
R(y)
10
1
10^{-1}
-6 -4 -2 0 2 4 6
y
negative particles
Au – DPM
Al---DPM
K
b)
π
R(y)
10
1
10^{-1}
-6 -4 -2 0 2 4 6
y

Fig. 4

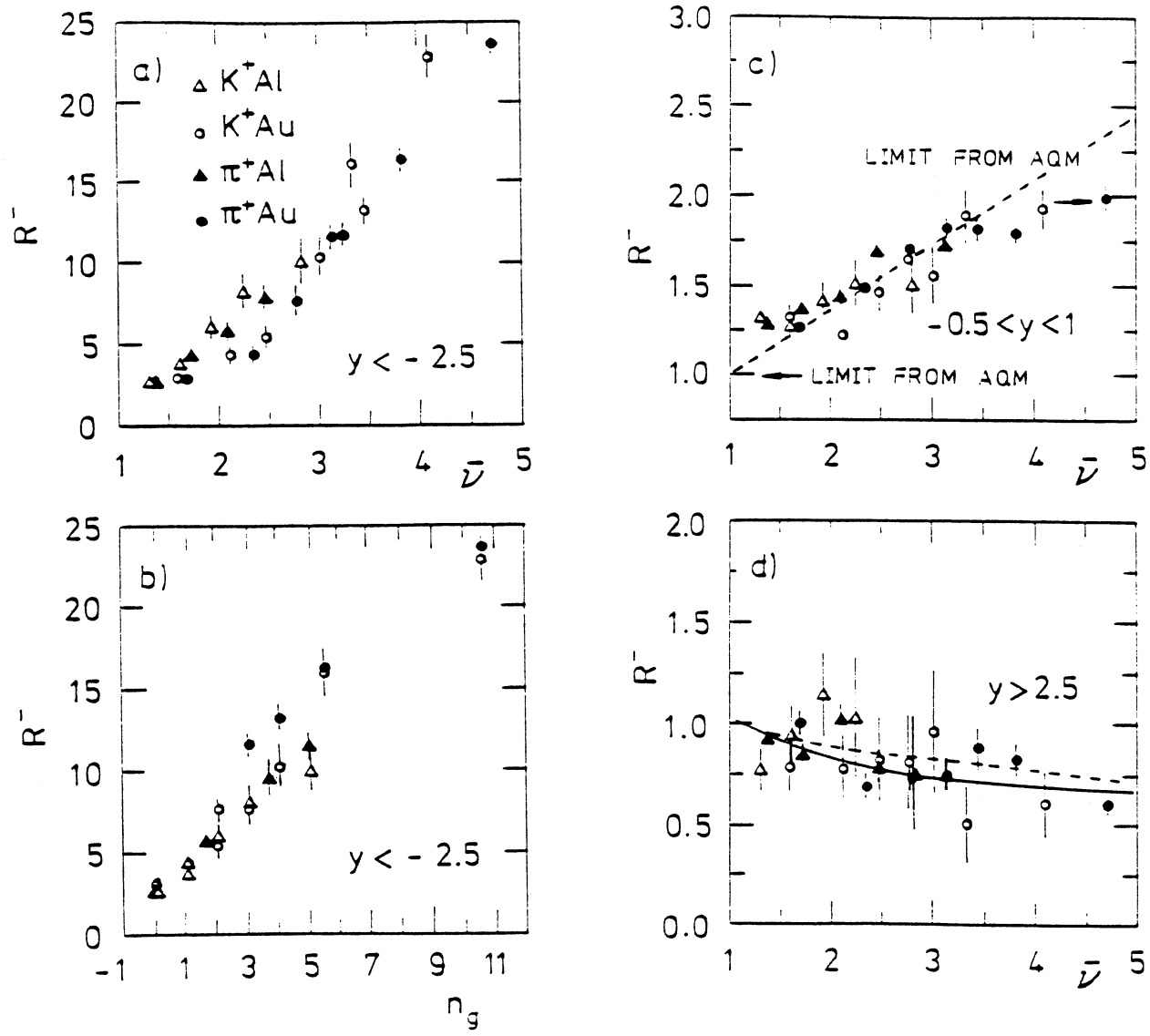
a)
Δ K⁺Al
o K⁺Au
▲ π⁺Al
● π⁺Au
y < - 2.5
R⁻
$\bar{\nu}$
b)
y < - 2.5
R⁻
n_g
c)
LIMIT FROM AQM
-0.5<y<1
LIMIT FROM AQM
R⁻
$\bar{\nu}$
d)
y>2.5
R⁻
$\bar{\nu}$

Fig. 5

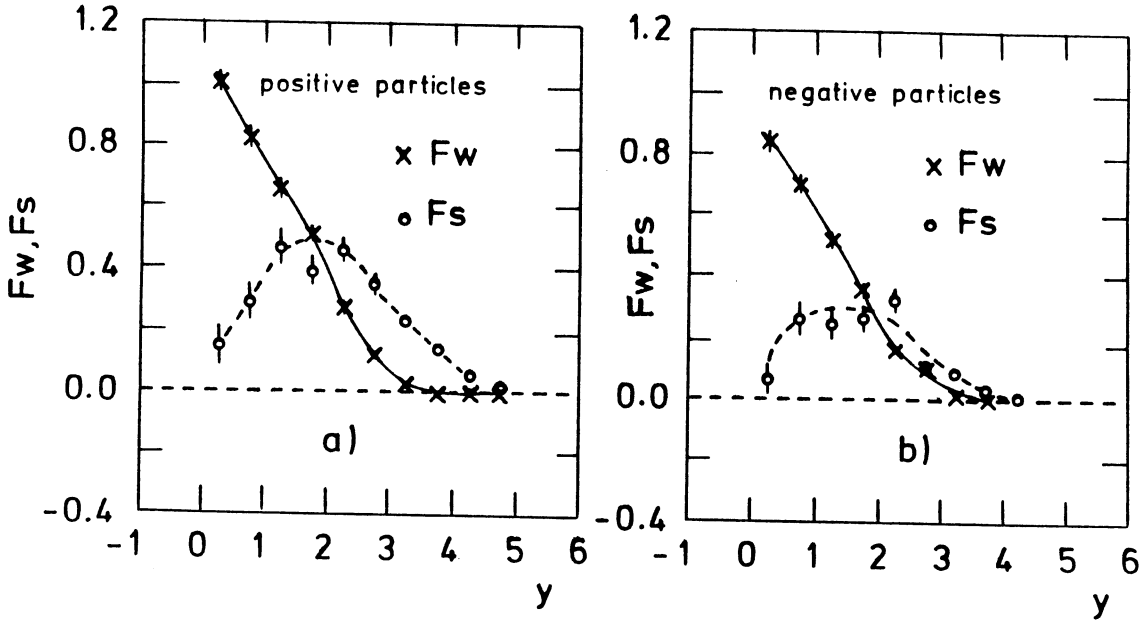
positive particles
x Fw
o Fs
a)
negative particles
x Fw
o Fs
b)
Fw, Fs
y

Fig. 6

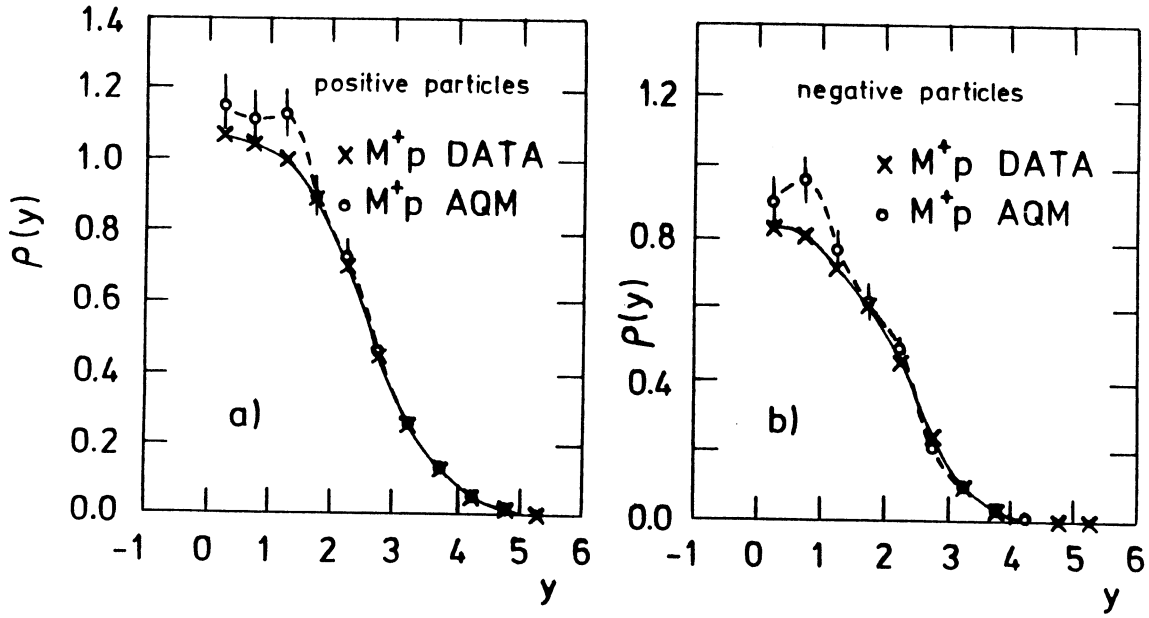
positive particles
x M⁺p DATA
o M⁺p AQM
a)
negative particles
x M⁺p DATA
o M⁺p AQM
b)
ρ(y)
y

Fig. 7

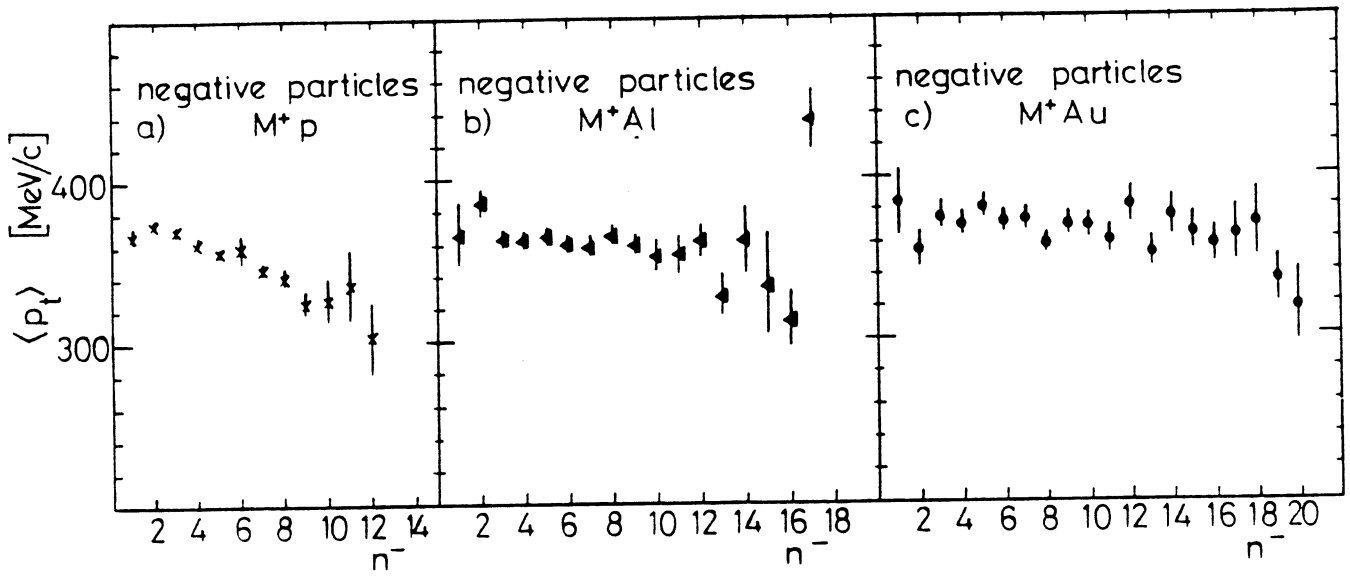
negative particles
a) M⁺ p
negative particles
b) M⁺ Al
negative particles
c) M⁺ Au
⟨p_t⟩ [MeV/c]
400
300
2 4 6 8 10 12 14
n⁻
2 4 6 8 10 12 14 16 18
n⁻
2 4 6 8 10 12 14 16 18 20
n⁻

Fig. 8

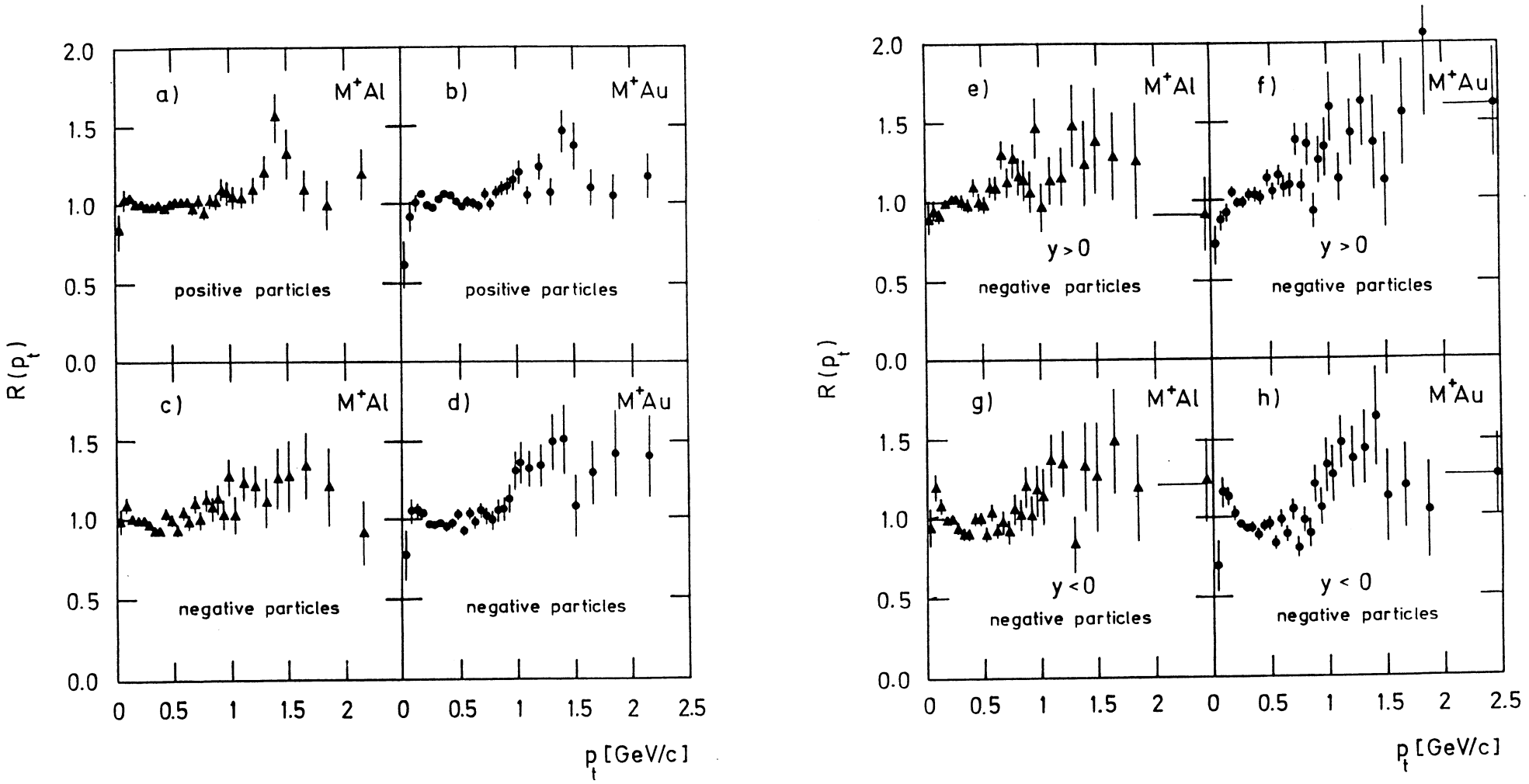
a)
M+Al
positive particles
b)
M+Au
positive particles
c)
M+Al
negative particles
d)
M+Au
negative particles
e)
M+Al
y > 0
negative particles
f)
M+Au
y > 0
negative particles
g)
M+Al
y < 0
negative particles
h)
M+Au
y < 0
negative particles
R(pt)
pt [GeV/c]

Fig. 9

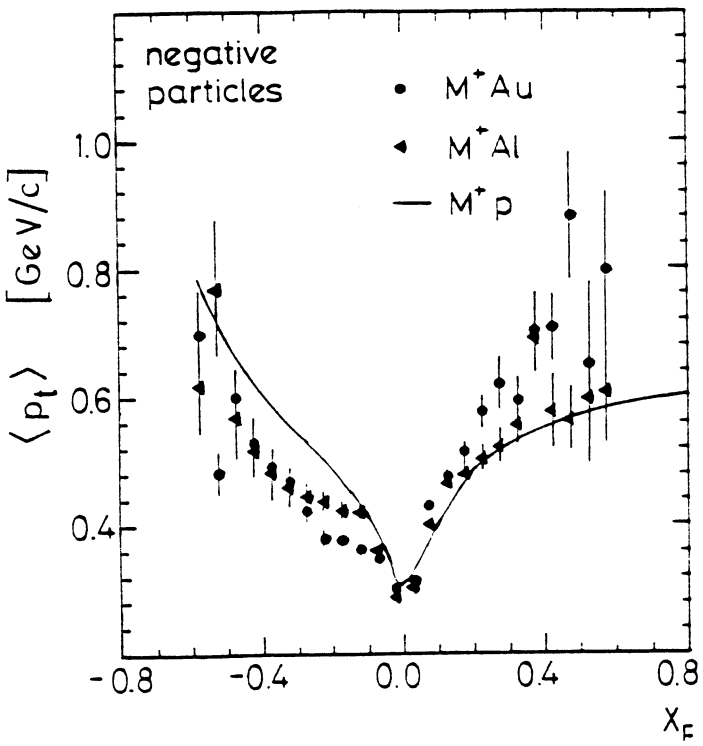
negative
particles
M⁺Au
M⁺Al
M⁺p
⟨pt⟩ [GeV/c]
1.0
0.8
0.6
0.4
-0.8
-0.4
0.0
0.4
0.8
XF

Fig. 10

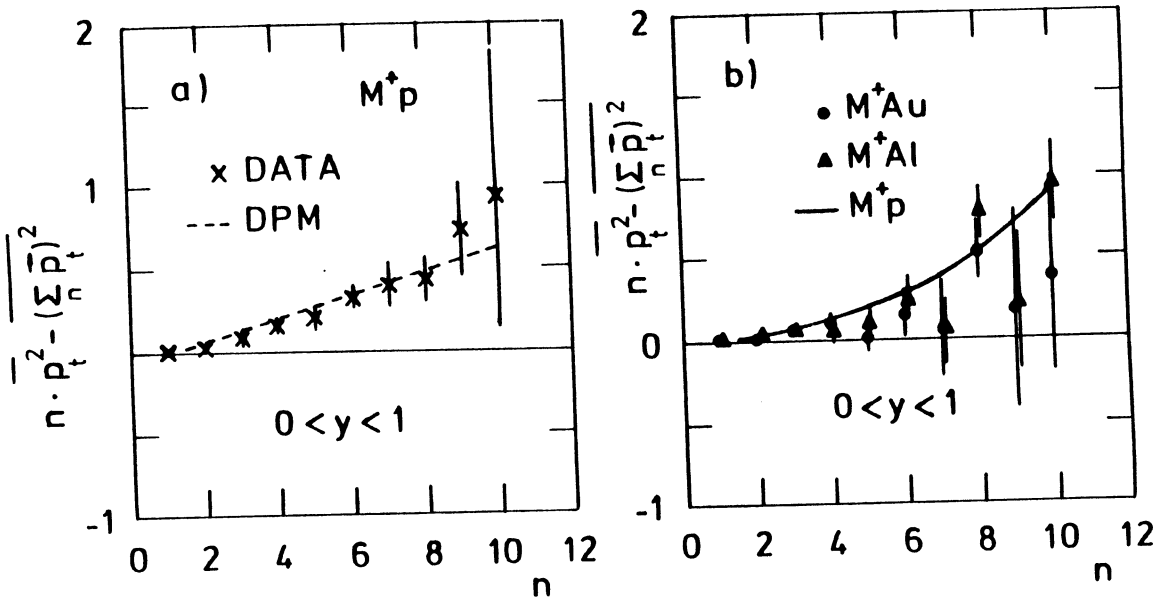

Fig. 11

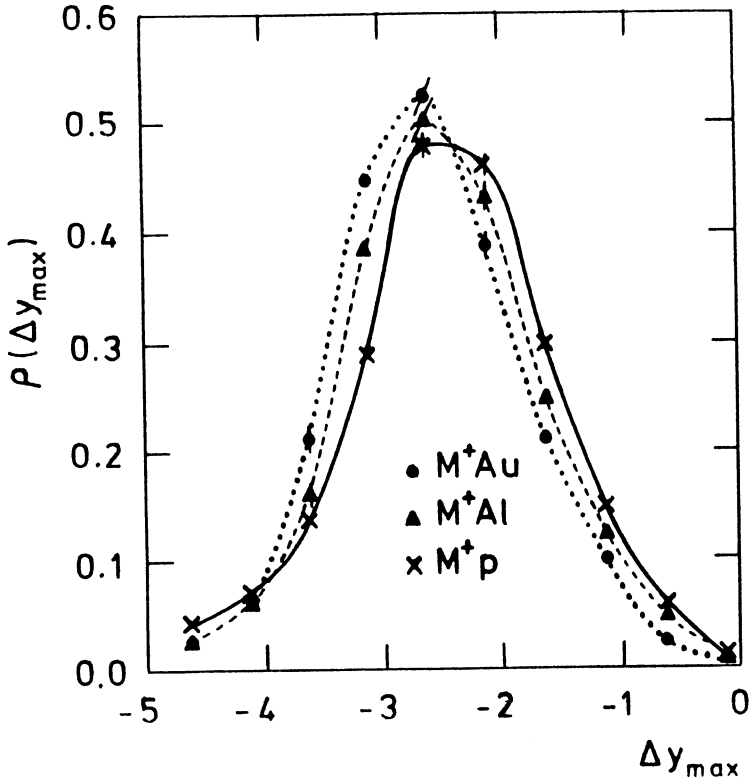
0.6
0.5
0.4
0.3
0.2
0.1
0.0
$\rho(\Delta y_{max})$
M⁺Au
M⁺Al
M⁺p
-5
-4
-3
-2
-1
0
Δy_{max}

Fig. 12

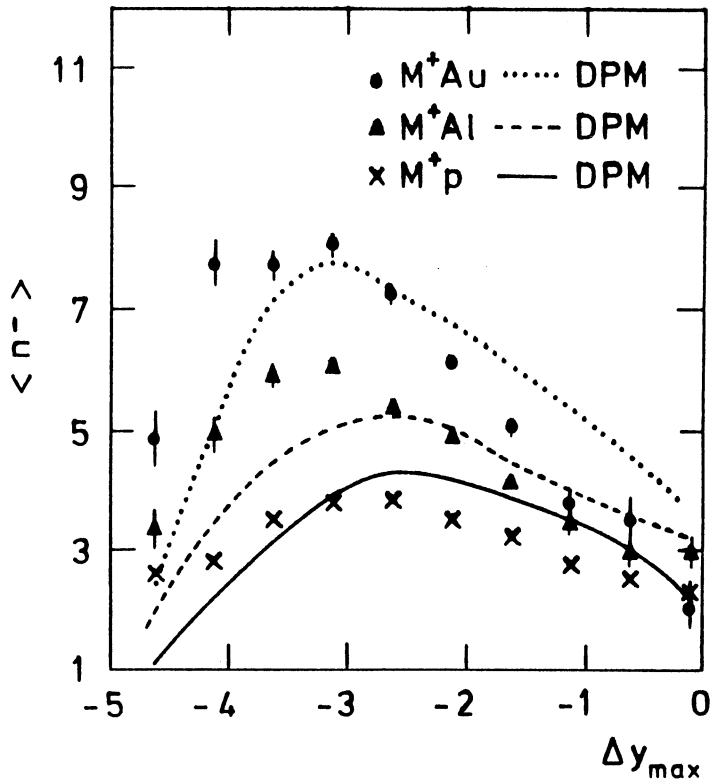
11
9
7
5
3
1
$\langle n \rangle$
M⁺Au ····· DPM
M⁺Al ---- DPM
M⁺p —— DPM
-5
-4
-3
-2
-1
0
Δy_{max}

Fig. 13

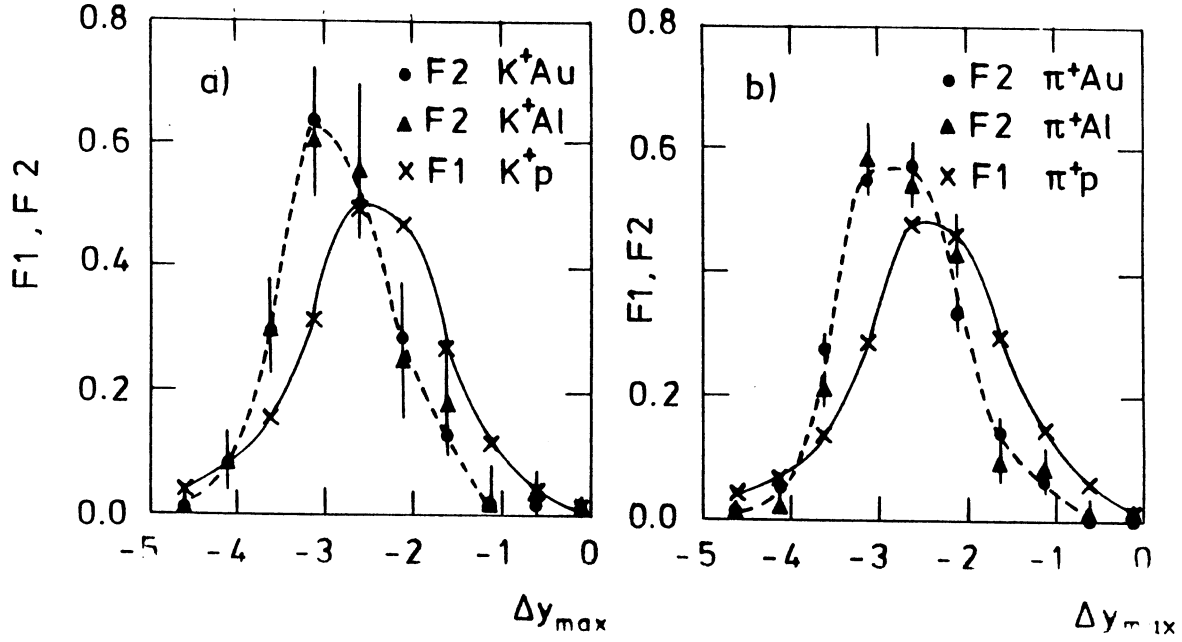
a)
• F2 K⁺Au
▲ F2 K⁺Al
× F1 K⁺p
b)
• F2 π⁺Au
▲ F2 π⁺Al
× F1 π⁺p
F1, F2
Δy_max

Fig. 14

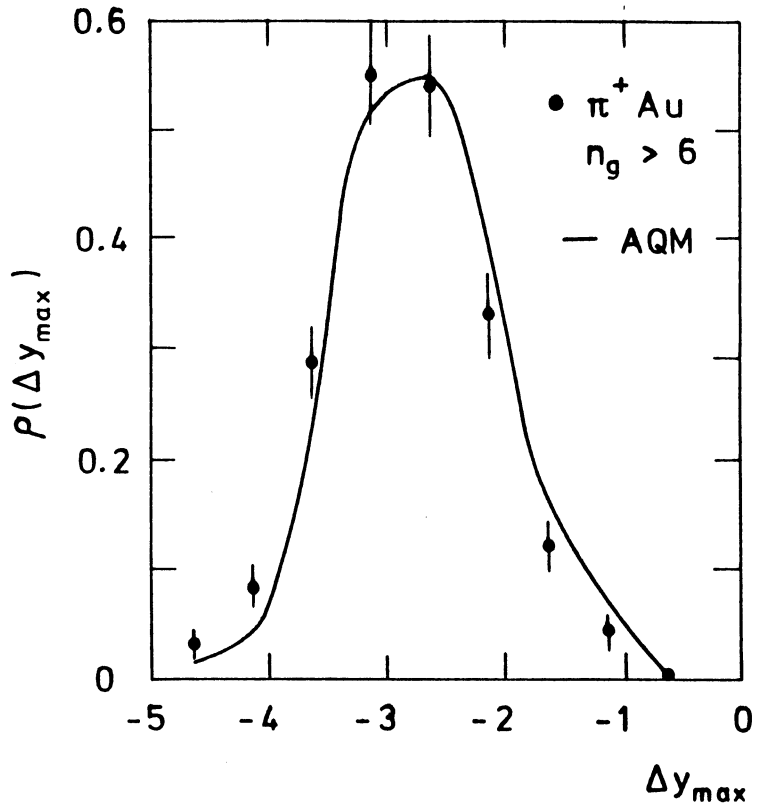
• π⁺Au
n_g > 6
— AQM
ρ(Δy_max)
Δy_max

Fig. 15

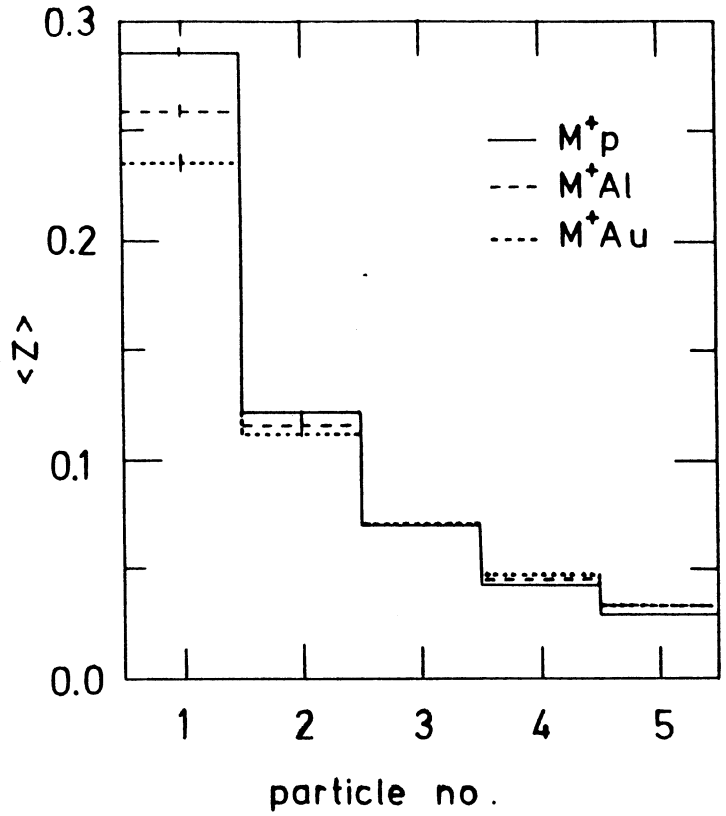

Fig. 16